ELSEVIER

Coordination Chemistry Reviews
185–186 (1999) 629–651

COORDINATION CHEMISTRY REVIEWS

Electronic structure of transition metal complex-based molecular metals and superconductors

Enric Canadell *

Institut de Ciència de Materials de Barcelona (CSIC), Campus de la UAB, 08193 Bellaterra, Spain

Received in revised form 4 December 1998; accepted 4 December 1998

Contents

Abstract

The electronic structure of some transition metal complex-based molecular solids is analyzed in order to discuss why the use of transition metal complexes can provide interesting new low-dimensional molecular conductors. The molecular solids considered include several charge transfer salts of both M $(dmit)_2$ (M=Ni, Pd, Pt) acceptors and M $(dddt)_2$ (M=Ni, Pd, Pt) donors.

Keywords: Molecular conductors; Electronic structure; Band structure

* Tel.: + 34-93-5801853; fax: + 34-93-5805729.
E-mail address: canadell@icmab.es (E. Canadell)

0010-8545/99/$ - see front matter
PII: S0010-8545(99)00015-6

1. Introduction

The unusual properties of molecular metals based on transition metal complex anions like $[Pt(CN)_4]$ or $[Pt(C_2O_4)_2]$ were studied actively in the late sixties and beginning of the seventies [1]. All of these materials were shown to undergo a metal to insulator transition at low temperature so that superconductivity could not be achieved. The synthesis of the first organic molecular metal, TTF-TCNQ (TTF: tetrathiafulvalene, TCNQ: tetracyanoquinodimethane), in 1973 [2] and the subsequent discovery of superconductivity in $(TMTSF)_2PF_6$ (TMTSF: tetramethyltetraselenafulvalene) in 1980 [3], shifted the attention of most of the low - dimensional molecular solid state community towards the potential of organic molecules related to TTF. Since then a quite impressive number of molecular conductors-which have led to superconductivity and a wealth of new fundamental phenomena [4]—have been prepared using organic donor molecules like TMTSF or BEDT-TTF (bis(ethylenedithio(tetrathiafulvalene)).

The discovery in 1986 of the first superconducting charge transfer salt containing a transition metal complex [5], $TTF[Ni(dmit)_2]_2$ (dmit: 1,3-dithiol-2-thione-4,5-dithiolate), revived the interest in transition metal complexes as building blocks for new molecular conductors. After 12 years of quite intense effort, the initial expectations have been almost fulfilled completely. New molecular solids containing transition metal complexes have been found to exhibit superconductivity [6], coexistence of superconductivity and localized paramagnetic moments in a stoichiometric lattice [7], two-band behavior [8], etc. Of course, it is not possible to give a comprehensive overview of the electronic structure of transition metal complex-based molecular conductors and superconductors in a limited space such as that of the present work. Here, we have rather tried to highlight why transition metal complexes can provide interesting new results in the field of low-dimensional molecular conductors. In the following, we will first review some basic ideas concerning the electronic structure of molecular conductors, and later, we will consider some examples of transition metal complex-based molecular conductors exhibiting distinctive features in their electronic structure with respect to those based on organic molecules.

2. Electronic structure of molecular metals

2.1. Basic concepts

The electronic structure of molecular metals is usually discussed in terms of band theory [9]. In order to briefly introduce the basic terminology [10] we will use in our discussion, let us consider a rectangular two-dimensional (2D) lattice with repeat vectors a and b as shown in Fig. 1a. Each lattice site may be assumed to have one orbital and one electron. Under the approximation of nearest neighbor interactions and the neglect of overlap integrals, the electronic energies allowed for the 2D lattice are written as $e(k_a, k_b) = \alpha + 2\beta_a \cos(k_a a) + 2\beta_b \cos(k_b b)$, where α is the energy of the site orbital, and β_a and β_b are the nearest neighbor transfer integrals

along the a- and b-directions, respectively. The wave vectors $k \equiv (k_a, k_b)$ can have any value within the first Brillouin zone defined by $-a^*/2 \leq k_a \leq a^*/2$ and $-b^*/2 \leq k_b \leq b^*/2$ (see Fig. 1b where $\Gamma = (0, 0)$, $X = (a^*/2, 0)$ and $Y = (0, b^*/2)$, $a^* = 2\pi/a$ and $b^* = 2\pi/b$). For the rectangular 2D lattice, the directions of the reciprocal vectors a^* and b^* are the same as those of the repeat vectors a and b, respectively. The difference between two successive $e(k_a, k_b)$ values is very small so that the complete set of energies given by the previous equation is a continuous set of energy levels called a band.

In the context of one-electron band theory, where electron-electron repulsion is neglected so that each band level can be filled with two electrons, a metal is defined as a system which has at least one partially filled band. Thus, there is no energy gap between the highest occupied level (i.e. the Fermi level e_f) and the lowest unoccupied level. Suppose that the 2D lattice represents an ideal one-dimensional (1D) system so that $\beta_a \neq 0$ and $\beta_b = 0$. That is, there is no intersite interaction along the b-direction, and so the 2D lattice is an assembly of non interacting chains running along the a-direction. Then, the $e(k)$ versus k plot is dispersive along the chain direction (see $\Gamma \rightarrow X$) but dispersionless along the interchain direction (see $\Gamma \rightarrow Y$), as illustrated in Fig. 1c. With one electron per site the bottom half of the allowed energy levels are each doubly occupied to form a metallic state (the dashed line in Fig. 1c represents the Fermi level). For a 2D lattice with non negligible intersite interactions along both a and b (i.e. β_a, $\beta_b \neq 0$) the band will be dispersive along both a^* and b^*.

For a partially filled band, some of the wave vectors of the Brillouin zone are associated with occupied energy levels and some with unoccupied energy levels. The boundary surface separating the occupied wave vectors from unoccupied wave vectors is called the Fermi surface (of course, in a 2D representation one should

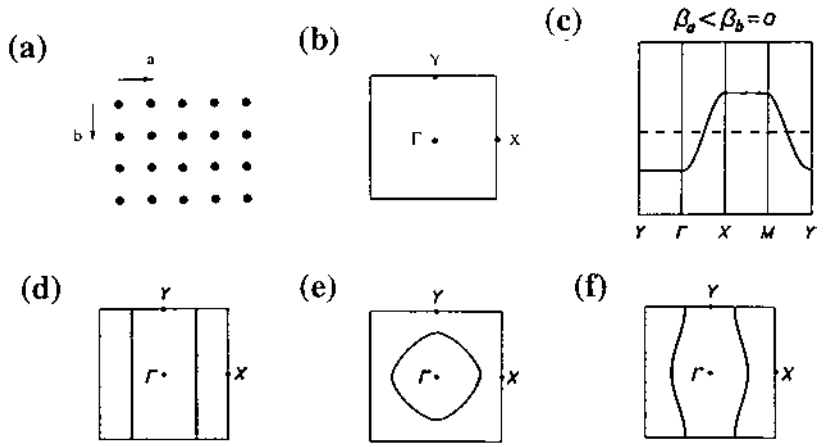

Fig. 1. Schematic representation of a rectangular lattice (a), its first Brillouin zone (b) and the band structure when $\beta_a \neq 0$ and $\beta_b = 0$ (c). In (d); (e) and (f) are shown schematically three different Fermi surfaces typical of 1D (d), 2D (e) and pseudo 1D (f) metals.

talk about a Fermi line). The Fermi surface associated with the half filled band of Fig. 1c is shown in Fig. 1d. It consists of two parallel lines perpendicular to the chain direction. Carriers of metals are those electrons at the Fermi level. When a certain wave vector direction does not cross the Fermi surface (e.g. $\Gamma \rightarrow Y$ in Fig. 1d) there are no electrons at the Fermi level having momentum along that direction so that the system is not metallic along that direction (i.e. the b direction in real space). The Fermi surface of Fig. 1d does not contain closed loops and hence corresponds to a 1D metal along the a direction. Depending on the relative values of the transfer integrals and thus, the dispersion of the bands along different directions, there are different types of Fermi surfaces. For instance, the Fermi surface can contain closed loops (see Fig. 1e) and then, the system is a 2D metal. The Fermi surface of Fig. 1f represents an intermediate situation, i.e. it is an open Fermi surface but with warped lines. It corresponds to a pseudo 1D metal along the a direction, i.e. a system with somewhat coupled chains along a.

In addition to the dimensionality of metallic properties, Fermi surfaces are also important in explaining the electronic instabilities of systems with partially filled bands [10]. When a piece of a Fermi surface can be translated by a vector q and superimposed on another piece of the Fermi surface, the Fermi surface is said to be nested by the vector q. An example of a perfectly nested Fermi surface is that of Fig. 1d. Metals with nested Fermi surfaces are susceptible towards a modulation with wave vector q of their charge or spin density, which destroys the nested portions of the Fermi surface. Thus, if the nesting is complete, after the appearance of the modulation the entire Fermi surface has been destroyed. The system exhibits a metal to insulator transition. If the nesting is only partial, part of the Fermi surface will remain after the appearance of the modulation and the transition will be of the metal to metal type. Metal to insulator transitions associated with such charge density or spin density waves are observed frequently at low temperature in 1D or pseudo 1D metals.

Finally, it must be recalled that our discussion has been limited to the case where a delocalized description of the electrons is valid. This is the case when the bandwidth (W) is large compared with the on-site repulsion (U). When $U > W$, the electrons prefer to be localized on lattice sites [11]. In that case the conductivity is activated because electron hopping from one site to the other leads to a situation in which two electrons reside on a single site, thereby causing on-site repulsion. Thus, if the dispersion of the band in Fig. 1c is small compared with the on-site repulsion, the system will prefer to have one electron localized in each site of the lattice and it will be a semiconductor. In some low-dimensional metals the bandwidth and on-site repulsion are comparable so that there can be a competition between the delocalized (i.e. metallic) and localized (i.e. semiconducting) electronic states. In that case, at a certain temperature the metallic system can undergo a metal to semiconductor transition which is different in nature from those discussed before. Disorder, throughout the random potential it introduces, is another important factor favoring localized states in low-dimensional metals and more specially in molecular conductors.

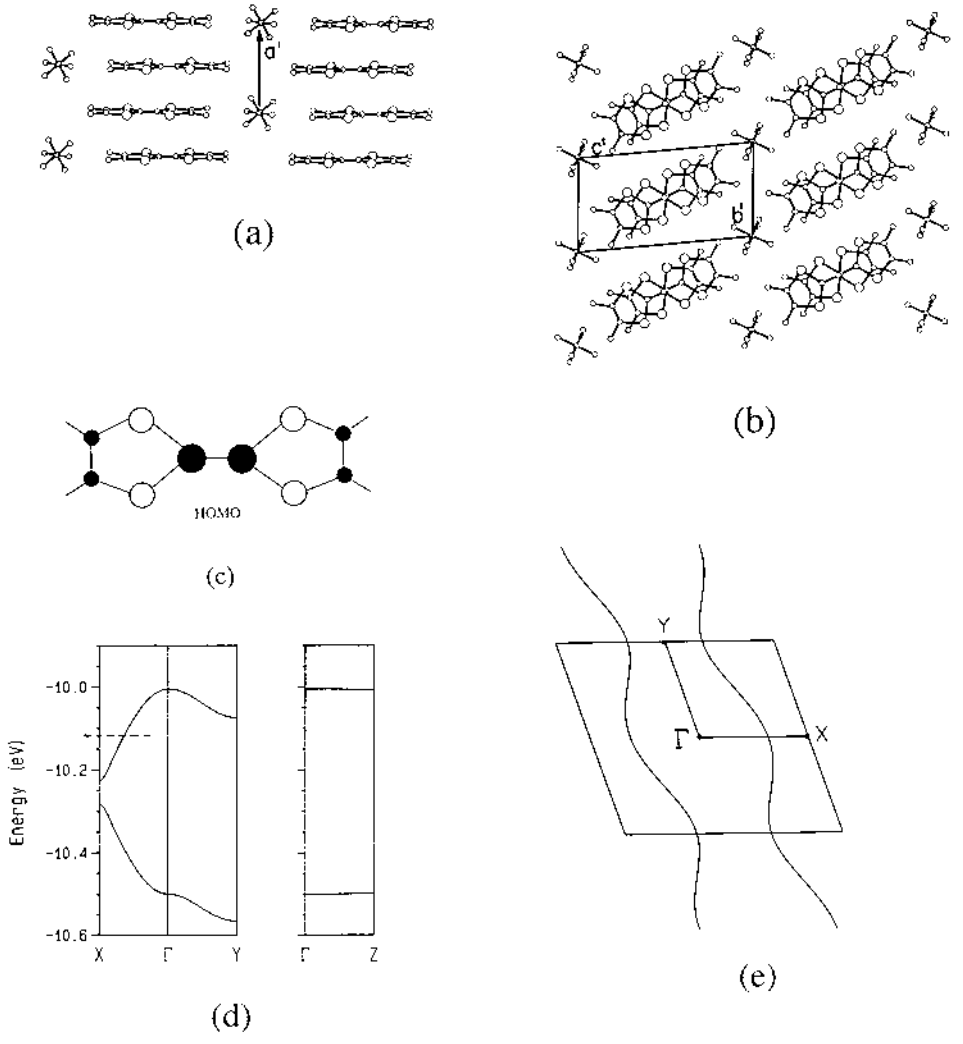

Fig. 2. Crystal structure of $(TMTSF)_2PF_6$ (a) and (b). Schematic representation of the HOMO of TMTSF (c). Calculated band structure (d) and Fermi surface for $(TMTSF)_2PF_6$. The dashed line in (d) denotes the Fermi level. Γ, X, Y and Z refer to the wave vectors (0, 0, 0); ($a^*/2$, 0, 0); (0, $b^*/2$, 0) and (0, 0, $c^*/2$), respectively.

2.2. Molecular metals

It is not difficult to see how the previous discussion can be directly used to understand the electronic structure of molecular metals. The only difference is that there will be several orbitals per unit cell and thus several bands. A band is full when there are two electrons per unit cell to fill this band. Let us consider the case of $(TMTSF)_2PF_6$. The crystal structure is shown in Fig. 2a and b [12]. It contains

layers of the TMTSF donors separated by layers of isolated PF_6 acceptors. Since the PF_6 anions are isolated their energy levels can not lead to energy bands. In contrast, there are many donor···donor interactions (mainly through short Se···Se contacts) which can lead to the formation of energy bands based on the TMTSF π-type molecular orbitals. Because of the molecular nature of charge transfer salts, the intermolecular interactions leading to the spread of the molecular energy levels into bands are weaker than the intramolecular chemical bonding forces which determine the molecular energy levels of the donor and the acceptor. Consequently, the highest occupied energy band of this salt (which in fact will be filled partially as a result of the charge transfer) should be adequately described by considering just the highest occupied molecular orbital (HOMO) of TMTSF. Because of the stoichiometry, one electron every two TMTSF molecules is transferred to PF_6 so that the TMTSF donors have an average charge of $+\frac{1}{2}$. This means that the HOMO band(s) should be filled partially and thus, if the HOMO of TMTSF is engaged in HOMO···HOMO interactions through the crystal, leading to the formation of dispersive HOMO band(s), the $(TMTSF)_2PF_6$ salt could be metallic.

The HOMO of TMTSF is shown schematically in Fig. 2c. It is a π-type orbital with strong contributions from the sulfur p orbitals. Thus, the overlap between HOMO orbitals of adjacent TMTSF donors along the chain direction of the crystal (see Fig. 2b) will be important. Since the unit cell of the salt contains two TMTSF donors, two HOMO combinations can be formed and every one of them will lead to an energy band through interactions between unit cells. These two bands should be filled with only three electrons because of the charge transfer and thus, at least one of them should be filled partially. The calculated band structure in the region of the Fermi level is shown in Fig. 2d where the dashed line refers to the Fermi level. As expected, the two bands shown there are almost build completely from the HOMO of the TMTSF donors and they are well separated from the other filled or unfilled energy bands. Since there are three electrons per unit cell to fill the two bands of Fig. 2d, the lower band is filled completely and the upper one is half-filled. What the band structure of Fig. 2d is also telling us is something about the strength of the HOMO···HOMO interactions along the crystal. For instance, the band dispersion along the chain direction (i.e. when changing the value of k from $\Gamma \equiv (0, 0, 0)$ to $X \equiv (a^*/2, 0, 0)$) is clearly stronger than the band dispersion along the interchain direction of the TMTSF layers (i.e. along $\Gamma \rightarrow Y$). The band dispersion along the interlayer direction (i.e. along $\Gamma \rightarrow Z$) is practically nil. These observations are easily understandable when taking into account the π-type nature of the HOMO and the details of the crystal structure.

Since the dispersion of the partially filled band is quite sizeable, $(TMTSF)_2PF_6$ should be a pseudo 1D metal with higher conductivity along the chain direction. This is in agreement with the calculated Fermi surface shown in Fig. 2e. This Fermi surface is open and contains warped lines approximately perpendicular to the chain direction. In addition, this Fermi surface is quite well nested. As a consequence, $(TMTSF)_2PF_6$ looses the metallic character at 12 K due to a spin density wave instability. The metallic character can however be restored under a pressure of 9 kbar and the salt becomes superconducting at 0.9 K [3].

It is important to emphasize that although there are two HOMO bands (because there are two donors per unit cell), only one orbital *per molecular species* is needed to describe the relevant part of the band structure (i.e. the levels near the Fermi level). Thus, these salts can be called *one-band systems*. Many of the presently known molecular conductors are indeed one-band systems.

The preceding discussion outlines some useful strategies that chemists can use in the search for new molecular conductors with interesting properties. Once a given structural type is known, one can try to modify the band structure by slightly changing some of the transfer integrals of the lattice (i.e. some of the intermolecular interactions). This can be realized by using slightly different counterions which through hydrogen bonding will induce modifications in the layers of the species responsible for the conductivity. Quite often, slight chemical changes can lead to strong changes in the transport properties. For instance, whereas the $(NHMe_3)[Ni(dmit)_2]_2$ salt is metallic, the strongly related $(NH_2Me_2)[Ni(dmit)_2]_2$ is semiconducting. The reasons for the different type of conductivity can be traced back to the subtle changes in the internal structure of the $Ni(dmit)_2$ stacks induced by the different counterions [13]. Another strategy is to change the number of electrons filling the bands. For instance, the trimerized TMTSF stacks in the two salts $(TMTSF)_3[Ti_2F_8(C_2O_4)]$ and $(TMTSF)_3Ta_2F_{11}$ are very similar [14,15]. However, whereas the second salt is a room temperature metal, the first one is semiconducting. This is a consequence of the different charge of the anions (-2 and -1, respectively). The unit cell of these salts contains three TMTSF donors and thus the band structure has three TMTSF HOMO bands [16]. Because of the trimerization these bands are well separated. In $(TMTSF)_3Ta_2F_{11}$ there are five electrons to fill the HOMO bands and thus, the upper band is half filled. This leads to the metallic behavior. However, in $(TMTSF)_3[Ti_2F_8(C_2O_4)]$, with only four electrons to fill the HOMO bands, the upper band is empty and, consequently, there is a band gap at the Fermi level. This leads to the semiconducting behavior.

3. Why transition metal complexes are interesting as building blocks for new molecular conductors?

In this section we will consider some examples of transition metal complex-based molecular conductors in which the transition metal complex is responsible for the conduction process and that exhibit original features in their electronic structures with respect to those based on organic molecules.

3.1. Two-band systems

For a long time it was assumed that charge transfer molecular conductors were *one-band systems* (see Section 2.2). This fact did not lead to serious problems in understanding their electronic structure and physical properties. The reason is that they were based mostly on organic molecules for which the HOMO–LUMO gap was relatively large. The energy splitting between the HOMO and LUMO of some

transition metal complexes can be much smaller than those of organic molecules. If the HOMO–LUMO energy splitting of one of the partners of the salt is comparable to the strength of the intermolecular interactions in which it is implicated, both the HOMO and LUMO of this molecule should be explicitly considered when building the band structure near the Fermi level. Thus, two types of bands associated with one of the partners of the charge transfer salt must be taken into account. Since two types of bands are associated with the *same* molecular species, these salts can be called *two-band systems* [17].

The first charge transfer salts which were proposed to be two-band systems [18] were α′-TTF[Pd(dmit)$_2$]$_2$ and TTF[Ni(dmit)$_2$]$_2$. The proposed two-band nature of these salts was consistent with X-ray diffuse scattering results [19] and was soon confirmed by ^{13}C Knight shift [20] and magnetic susceptibility [21] measurements. The HOMO and LUMO of an ideal M(dmit)$_2$ (M=Ni, Pd, Pt) unit (see Fig. 3a) are shown schematically in Fig. 4. They are built from in-phase and out-of-phase combinations of the same π-type orbital of the dmit ligand. Although the M d_{xz} orbital has the appropriate symmetry to mix into the LUMO, the nodal properties of the ligand orbital (i.e. different sign for the carbon and the sulfur z orbital contribution) are such that the overlap, and thus the mixing, is relatively weak. In addition, the d metal orbitals cannot mix into the HOMO because of the three symmetry planes. Consequently, the metal–ligand interactions cannot lead to a large HOMO–LUMO energy splitting (Δ). According to single-ζ extended Hückel calculations this splitting is around 0.4 eV [22]. As it will be shown in the following, this modest but however non negligible energy splitting lies at the heart of the two-band behavior of some charge transfer salts of the M(dmit)$_2$ acceptor [17,18,23].

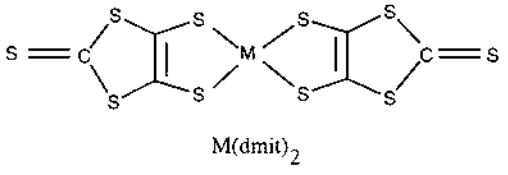

M(dmit)$_2$

(a)

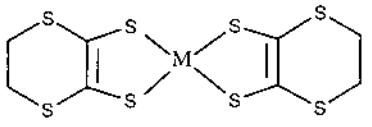

M(dddt)$_2$

(b)

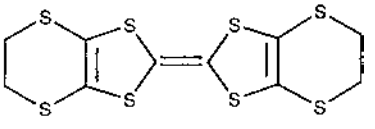

BEDT-TTF

(c)

Fig. 3. Some building blocks used in the construction of molecular solids: M(dmit)$_2$ (a), M(dddt)$_2$ (b) and BEDT-TTF (c).

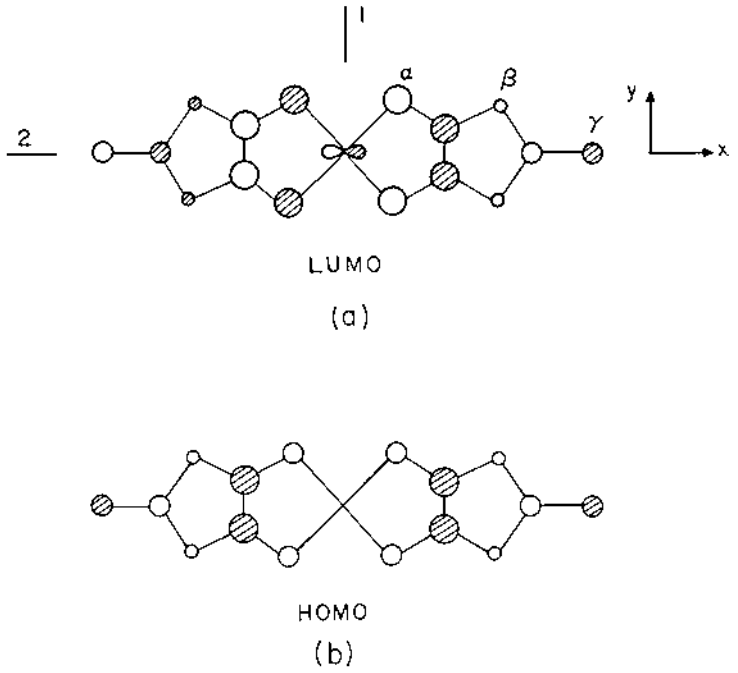

Fig. 4. LUMO and HOMO of an ideal $M(dmit)_2$ (M=Ni, Pd, Pt) molecule.

3.1.1. Salts containing uniform chains

Let us first consider the case of salts containing uniform chains of $M(dmit)_2$ units. This is the case of $TTF[Ni(dmit)_2]_2$ and α'-$TTF[Pd(dmit)_2]_2$ [24,25]. Despite being isostructural and room temperature metals, the two salts have different physical behavior at low temperature. $TTF[Ni(dmit)_2]_2$ is metallic down to 3 K at ambient pressure and becomes superconducting at 1.6 K under 7 kbar [26]. The α'-$TTF[Pd(dmit)_2]_2$ phase is metallic until around 220 K, exhibits activated conductivity below this temperature at ambient pressure, and becomes superconducting under 20 kbar at 6.5 K [27]. A puzzling question about $TTF[Ni(dmit)_2]_2$ was the existence of 1D structural instabilities in X-ray diffuse scattering experiment [19] while no major resistivity anomalies were observed. A similar X-ray study of α'-$TTF[Pd(dmit)_2]_2$ showed the existence of two sets of diffuse lines at the reduced wave vectors $q_1 = 0.5\ b^*$ and $q_2 = \pm 0.31\ b^*$. Such diffuse lines, related to two different charge density wave (CDW) instabilities of the acceptor stacks, condense into satellite reflections at 150 and 105 K, respectively [19]. At low temperatures additional satellite reflections at the reduced wave vectors $2q_2$ and $q_2 \pm q_1$ are also observed. The change in the conductivity regime observed below 220 K can thus be associated with the development of these CDW instabilities.

The crystal structure of $TTF[Ni(dmit)_2]_2$ and α'-$TTF[Pd(dmit)_2]_2$ is shown in Fig. 5 [24,25]. Slabs of $M(dmit)_2$ alternate with slabs of TTF. The $M(dmit)_2$ slabs are built from four stacks. There are four different types of intermolecular interactions

between $M(dmit)_2$ molecules of a slab. Those labeled 1, 2 and 9 involve lateral (interstacks) interactions. In addition, there is one interslabs $M(dmit)_2$–$M(dmit)_2$ interaction. The only short contacts between TTF molecules are those along the *b* direction. Finally, there are three different types of TTF–$M(dmit)_2$ interactions. As shown elsewhere [18], except for the $HOMO_{TTF}$–$HOMO_{TTF}$, $HOMO_{M(dmit)2}$–$HOMO_{M(dmit)2}$ and $LUMO_{M(dmit)2}$–$LUMO_{M(dmit)2}$ interactions along the *b* direction, all other interactions involving the $HOMO_{M(dmit)2}$, $LUMO_{M(dmit)2}$ or $HOMO_{TTF}$ are quite small. This leads to the strongly one-dimensional (1D) band structure shown in Fig. 6 for the $Pd(dmit)_2$ slabs of α′-$TTF[Pd(dmit)_2]_2$ [18]. The more surprising result of that Figure is that the four LUMO bands overlap with the four HOMO bands. As a consequence of the strong interactions along the *b* direction the band dispersion more than compensates for the initial HOMO–LUMO splitting and consequently, both the HOMO and LUMO bands are filled partially for reasonable electron transfers. This means that *there is an internal HOMO–LUMO electron transfer in addition to the usual donor–acceptor electron transfer*.

The resistivity measurements for $TTF[Pd(dmit)_2]_2$ [27] show that at low temperature there are no more carriers in the system. This can only be explained by the appearance of energy gaps at the Fermi level in all the conduction bands of the system: the HOMO and LUMO bands of $Pd(dmit)_2$ and the HOMO bands of TTF. As shown in Fig. 6, for any reasonable donor–acceptor charge transfer, the LUMO bands are cut near $k_F^{LUMO} \approx 0.25\ b^*$ and the HOMO bands near $k_F^{HOMO} \approx 0.15\ b^*$. Thus, because of the strong 1D nature of the band structure, it can be assumed that the LUMO bands are nested by $2k_F^{LUMO} = 0.5\ b^* = q_1$ and the HOMO bands are nested by $2k_F^{HOMO} = 0.31\ b^* = q_2$. However, the question is what does it happen

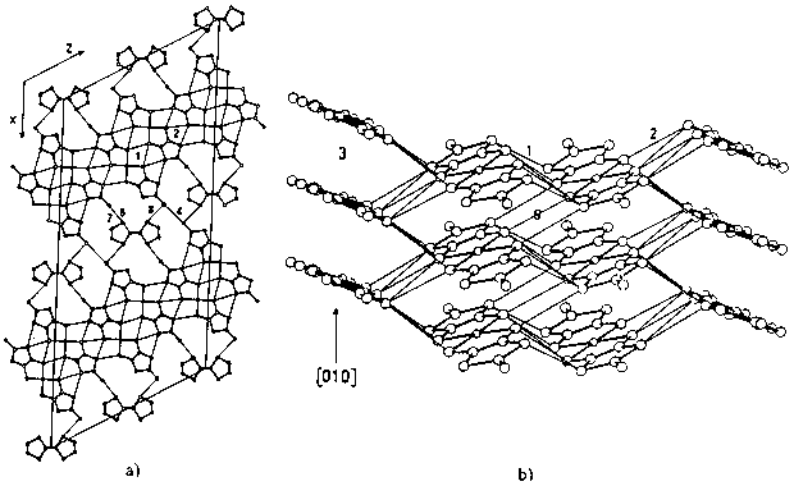

Fig. 5. Crystal structure of $TTF[Ni(dmit)_2]_2$ and α′-$TTF[Pd(dmit)_2]_2$: (a) projection onto the (010) plane, and (b) parallel view along [010] of the $M(dmit)_2$ slabs. Intermolecular S···S contacts shorter than 3.7 Å are also shown as thick lines.

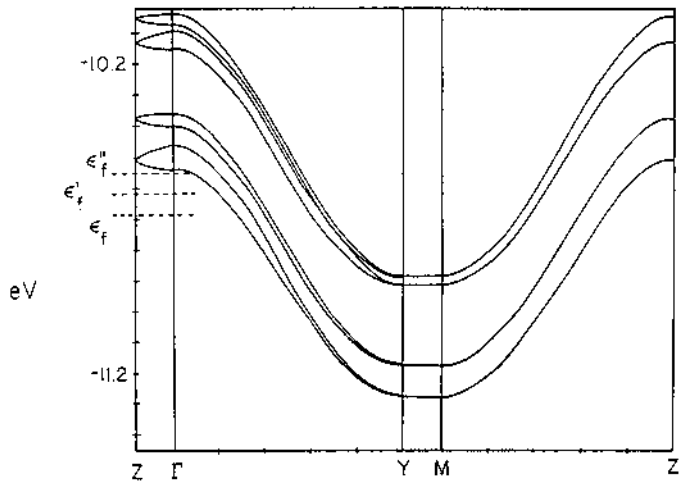

Fig. 6. Band structure of the $Pd(dmit)_2$ of α′-TTF[$Pd(dmit)_2$]$_2$. Γ, Y, Z and M refer to the wave vectors (0, 0); ($b^*/2$, 0); (0, $c^*/2$, 0) and ($b^*/2$, $c^*/2$), respectively. The Fermi levels noted ε_f, ε'_f and ε''_f are those appropriate for charge transfers of 0, 1/2 and 1 electrons per TTF, respectively. The four upper bands are the LUMO bands and the four lower bands are the HOMO bands.

with the carriers in the TTF HOMO bands? In such a 1D multi-band system with n bands, the charge transfer conservation rule is: $\Sigma\gamma_i\ (4k_F^i/b^*) =$ number of holes per unit cell (eight coming from the LUMO bands), where i refers to the different partially filled bands, γ_i is their degeneracy, and k_F^i is their Fermi wave vector. If we refer to the TTF HOMO Fermi wave vector as k_F^{TTF}, the charge conservation rule can be written, once the stoichiometry of the system is taken into account, as

$$4[(4k_F^{HOMO})/b^*] + 4[(4k_F^{LUMO})/b^*] + 2[(4k_F^{TTF})/b^*] = 4 \times 2 = 8$$

From this equality a charge transfer $\rho = (4k_F^{TTF})/b^* = 0.76\ b^*$ is obtained. Consequently, a distortion at $b^* - 2k_F^{TTF} = b^* - 0.38\ b^* = 0.62\ b^* = 2q_2$, which is observed experimentally [19], will thus also induce a gap on the TTF HOMO bands, leading to the destruction of all the carriers. Thus, the proposed two-band behavior for $Pd(dmit)_2$ adequately explains the otherwise puzzling X-ray diffuse scattering and resistivity results for α′-TTF[$Pd(dmit)_2$]$_2$.

The calculated band structure for the $Ni(dmit)_2$ slabs of TTF[$Ni(dmit)_2$]$_2$ is shown in Fig. 7 [18]. It is very similar to the band structure of Fig. 6 except for an important difference: the dispersion of both the HOMO and LUMO bands is smaller. The X-ray diffuse scattering study of TTF[$Ni(dmit)_2$]$_2$ showed the existence of 1D structural fluctuations under the form of diffuse lines at the reduced wave vectors $\pm 0.4\ b^*$ which at ambient pressure condensate into satellite reflections at 40 K [19]. There are two additional diffuse lines of very weak intensity at the wave vectors 0.22 and 0.18 b^* which do not lead to satellite reflections down to 25 K [18]. Comparison of these values with the band structure of Fig. 6, suggests that the three sets of instabilities can be attributed to the LUMO bands, the two upper

HOMO bands, and the two lower HOMO bands, respectively. The more puzzling fact about TTF[Ni(dmit)$_2$]$_2$ is that these instabilities have practically no effect on the resistivity. However it must be recalled that two of the 1D structural fluctuations do not condensate into satellite reflections. Although at present time this fact is not understood completely, it should be noted that according to the band structure of Fig. 7, the nesting of the HOMO bands is not as good as for α'-TTF[Pd(dmit)$_2$]$_2$. In fact, for charge transfers between 0.5 and 1, the Fermi surface of the bottom pair of HOMO bands is closed [28]. This is a consequence of the lower dispersion of the bands which places the Fermi level near the top of the HOMO bands. Another consequence of the smaller band dispersion is that the $2k_F$ wave vector of the LUMO bands changes from 0.5, leading to a commensurate modulation, to 0.4, leading to an incommensurate modulation. The two factors should make less favorable the condensation of the 1D structural instabilities in TTF[Ni(dmit)$_2$]$_2$. It has also been suggested that weak electron correlations as well as very weak electron–phonon coupling can be at the origin of the absence of a noticeable effect of the structural instabilities in the resistivity [29]. Whatever the reasons for this intriguing difference are, it is clear that the band structures of Figs. 6 and 7 [18] are completely consistent with the X-ray diffuse scattering studies [19]. The two-band behavior of TTF[Ni(dmit)$_2$]$_2$ and α'-TTF[Pd(dmit)$_2$]$_2$ was soon confirmed by ^{13}C Knight shift [20] and magnetic susceptibility studies [21].

Both TTF[Ni(dmit)$_2$]$_2$ and α'-TTF[Pd(dmit)$_2$]$_2$ exhibit a very rich phase diagram related to their two-band behavior [26,27]. One of the reasons is that the internal electron transfer between the HOMO and LUMO bands of the M(dmit)$_2$ slabs can be changed by temperature and pressure, leading to changes in the physical behavior. Although at first sight it could be thought that charge transfer salts of any square planar transition metal dithiolene molecule with M=Ni, Pd or Pt could

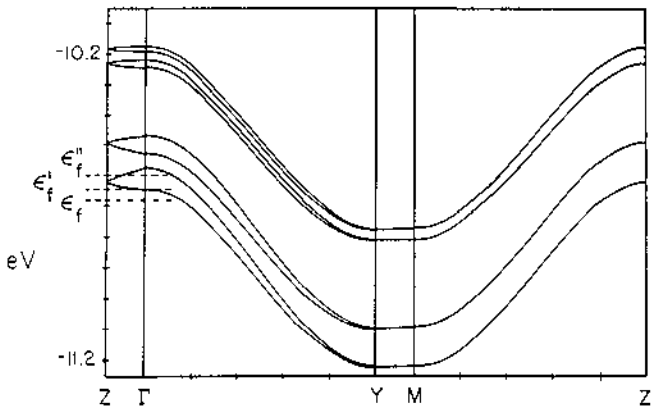

Fig. 7. Band structure of the Ni(dmit)$_2$ of TTF[Ni(dmit)$_2$]$_2$. *Γ*, *Y*, *Z* and *M* refer to the wave vectors (0, 0); (b*/2, 0); (0, c*/2, 0) and (b*/2, c*/2), respectively. The Fermi levels noted ε_f, ε'_f and ε''_f are those appropriate for charge transfers of 0, 1/2 and 1 electrons per TTF, respectively. The four upper bands are the LUMO bands and the four lower bands are the HOMO bands.

exhibit such a behavior, this is not the case. There are strong electronic and structural requirements which have been examined in detail elsewhere [8]. It is important to point out that the internal electron transfer associated with the two-band behavior has not been observed so far in organic charge transfer salts.

3.1.2. Salts containing slabs with dimeric building blocks

The internal electron transfer explored in the previous section is not the only unusual aspect of the two-band molecular conductors. Another interesting situation occurs in charge transfer salts containing slabs of the potentially two-band molecule with dimeric building blocks. All along this section the term 'dimeric building block' will not refer to the existence of real 'dimers' but to the fact that the unit cell of the slab contains two monomers. How strongly the two monomers interact, leading to real dimers or not, has a strong effect of the electronic structure of these salts.

A large number of salts like $NHMe_3[Ni(dmit)_2]_2$ [13], $NMe_4[Pt(dmit)_2]_2$ [30], $NMe_4[Ni(dmit)_2]_2$ [31], δ-TTF$[Pd(dmit)_2]_2$ [25], (EDT-TTF)$_2[Pd(dmit)_2]_2$ [32] or $Cs[Pd(dmit)_2]_2$ [33] contain $M(dmit)_2$ slabs in between donor slabs. Although there are differences in detail, the building blocks of these slabs contain two monomer units. Because of the presence of two monomers per repeat unit, the $M(dmit)_2$ HOMO and LUMO will generate two combinations: one bonding and one antibonding. Since the initial HOMO–LUMO splitting (Δ) is relatively small, there are two different possibilities concerning the ordering of the different energy levels of the dimer (see Fig. 8). First, if the transfer integrals (t_{HOMO} and t_{LUMO}) are smaller than Δ/2, the antibonding combination of the HOMO's (Ψ^-_{HOMO}) will be *lower* than the bonding combination of the LUMO's (Ψ^+_{LUMO}). Second, if the transfer integrals are greater than Δ/2, the antibonding combination of the HOMO's (Ψ^-_{HOMO}) will be *higher* than the bonding combination of the LUMO's (Ψ^+_{LUMO}). Shown in Fig. 8 are the HOMO and LUMO levels of the monomer and dimer of $M(dmit)_2$ as calculated for $NMe_4[Ni(dmit)_2]_2$ and $Cs[Pd(dmit)_2]_2$, respectively [23] Whereas the two HOMO combinations are kept lower than the two LUMO ones in $NMe_4[Ni(dmit)_2]_2$, this is not the case for $Cs[Pd(dmit)_2]_2$. Because of the stoichiometry, there are five electrons to fill these levels and consequently, the singly occupied level is the Ψ^+_{LUMO} in the first case but the Ψ^-_{HOMO} in the second case.

The calculated band structures for the acceptor slabs of $NMe_4[Ni(dmit)_2]_2$ and $Cs[Pd(dmit)_2]_2$ are reported in Figs. 9 and 10, respectively. As shown there, the interdimer interactions do not change the relative ordering of the dimer levels. In consequence, *the partially filled band of the $NMe_4[Ni(dmit)_2]_2$ salt is mainly built from the LUMO of the acceptor, as intuitively expected, but that of the $Cs[Pd(dmit)_2]_2$ salt is almost exclusively built from the HOMO of the acceptor, contrary to the intuitive reasoning*. Similar counterintuitive behavior is found in δ-TTF$[Pd(dmit)_2]_2$, (EDT-TTF)$_2[Pd(dmit)_2]_2$, (n-$Bu_4N)[Pd(dmit)_2]_2$ or $NMe_4[Pt(dmit)_2]_2$.

Although the inversion of the Ψ^-_{HOMO} and Ψ^+_{LUMO} levels in some salts can be surprising, optical data measurements [33,34] confirm it. Such inversion —first noticed for δ-TTF$[Pd(dmit)_2]_2$ [18]— must be related to some fundamental detail of

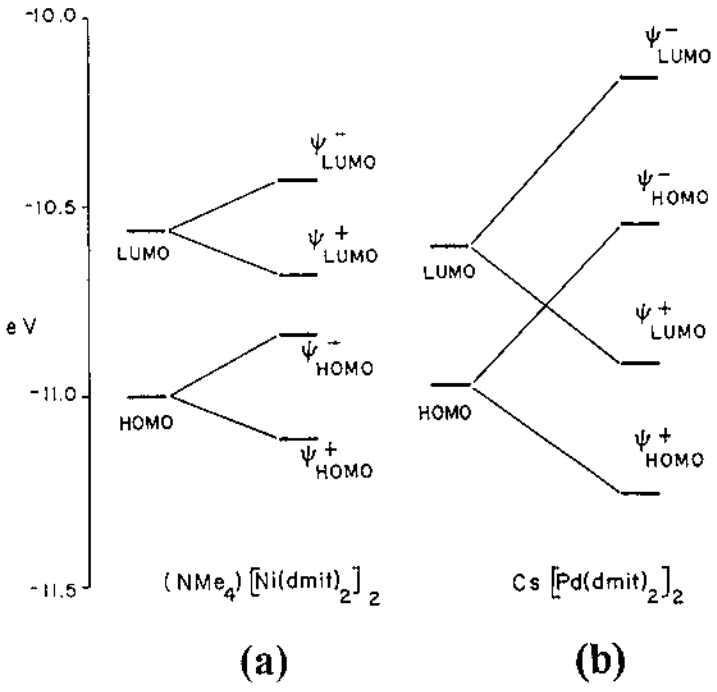

Fig. 8. HOMO and LUMO levels for the $M(dmit)_2$ monomer and $[M(dmit)_2]_2$ dimer as found in the room temperature structure of: (a) $NMe_4[Ni(dmit)_2]_2$, and (b) $Cs[Pd(dmit)_2]_2$.

the crystal structure. In order to clarify this point we need to consider the different modes of overlap between pairs of $M(dmit)_2$ units within the slabs. A careful analysis shows that the main difference resides in the intradimer type of overlap. It is of the atom-over-atom type in $Cs[Pd(dmit)_2]_2$ (see Fig. 11a) but slipped in $NMe_4[Ni(dmit)_2]_2$ (see Fig. 11b). The intradimer transfer integrals (t_{HOMO} and t_{LUMO}) are much larger in the first case because of the very favorable sulfur-over-sulfur overlap.

The obvious question now is why such a difference? In principle, the nature of both the donor and the metal could be responsible. The fact that very different donors like Cs, TTF, Me_4N and n-Bu_4N lead to the same type of intradimer overlap mode for the $Pd(dmit)_2$ salts, and that the same donor, Me_4N, leads to different intradimer overlap modes for the $Pd(dmit)_2$ and $Ni(dmit)_2$ salts, suggests that it is the nature of the metal atom which plays the leading role in determining the intradimer overlap. This is the result of the competition between two different contributions. First, we note that the LUMO of the monomer contains some contribution of the M d_{xz} orbital (see Fig. 4). In consequence, the Ψ^{+}_{LUMO} level of the dimer has some metal-metal bonding character. If there is no inversion between the Ψ^{-}_{HOMO} and Ψ^{+}_{LUMO} (Fig. 8a), then there is only one electron in the Ψ^{+}_{LUMO}. In that case the associated metal–metal bonding is weak. If the monomer–monomer interaction can be increased such that the inversion of the two levels occurs (Fig.

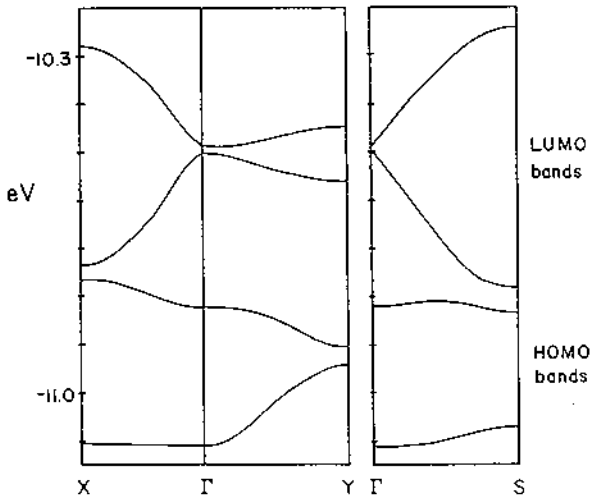

Fig. 9. Band structure for the $Ni(dmit)_2$ slabs in $NMe_4[Ni(dmit)_2]_2$. Γ, X, Y and S refer to the wave vectors (0,0); $(a_0^*/2, 0)$; $(0, b_0^*/2)$ and $(-a_0^*/2, b_0^*/2)$, respectively, where a_0 and b_0 are the primitive vectors defined as $a_0 = (a+b)/2$ and $b_0 = -b$.

8b), the metal–metal stabilization will be stronger because of both the double occupancy of Ψ^+_{LUMO} and the larger overlap between the metal centers. Optimization of the metal–metal bonding associated with Ψ^+_{LUMO} will lead to the atom-over-atom mode of overlap. The second contribution is due to the sulfur–sulfur repulsive interactions which arise from deeper levels not shown in Fig. 8. This repulsive contribution will be maximum for the atom-over-atom mode of overlap. Hence, it is clear that the intradimer mode of overlap will be the result of the

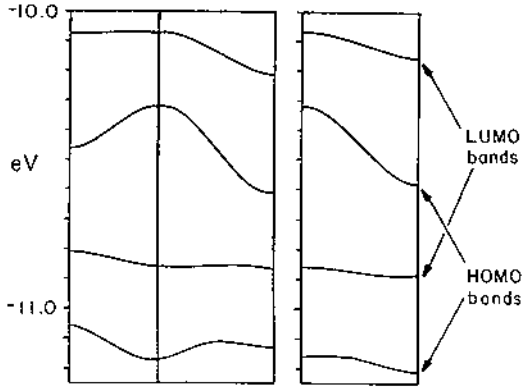

Fig. 10. Band structure for the $Pd(dmit)_2$ slabs in $Cs[Pd(dmit)_2]_2$. Γ, X, Y and S refer to the wave vectors (0,0); $(a_0^*/2, 0)$; $(0, b_0^*/2)$ and $(-a_0^*/2, b_0^*/2)$, respectively, where a_0 and b_0 are the primitive vectors defined as $a_0 = (a-b)/2$ and $b_0 = b$.

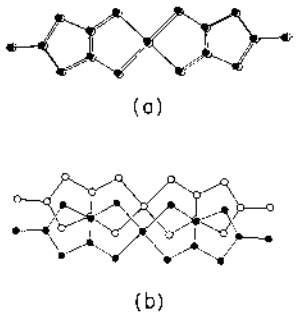

Fig. 11. Intradimer type of overlap in: (a) $Cs[Pd(dmit)_2]_2$ and (b) $NMe_4[Ni(dmit)_2]_2$.

tendency of the molecular pair to maximize the metal–metal bonding without increasing excessively the sulfur–sulfur repulsions. The relative strength of these two contributions will depend crucially on the spatial extension of the metal and sulfur orbitals. If this spatial extension is larger for the metal orbitals than for the sulfur ones, the stabilizing metal–metal interactions will be quite sizable for distances where the sulfur–sulfur repulsions are only small and the atom-over-atom configuration will be favored. This is certainly the case for the second and third period metal atoms Pd and Pt. If the spatial extension of the metal orbitals is smaller, as is the case for the first period atom Ni, the metal–metal stabilization will only be possible for distances where the sulfur–sulfur repulsions are already quite strong and the atom-over-atom configuration will not be favored.

The results of Fig. 9 and Fig. 10 are but two cases of a presumably smooth evolution of the band structure following the degree of dimerization and/or the nature of the interdimer interactions. The nature of the donor can play an important role here. Strong dimerization of the atom-over-atom type is expected for M=Pd and Pt but not for M=Ni. Thus, the influence of the cation is expected to be small for M=Pd and Pt. In this case the intradimer interactions will be dominated by the M···M interaction and the donor will mainly affect the interdimer interactions. However, the splitting between the Ψ^{+}_{LUMO} and Ψ^{-}_{HOMO} levels is quite sizable in all cases we have studied. Thus, changing the donor should not drastically change the position of the levels. We then believe that, although the nature of the donor can slightly tune the fine details of the band dispersion (and consequently, of the physical properties), for M=Pd and Pt the partially filled band will usually originate from the Ψ^{-}_{HOMO}. An interesting question here is the possible role of pressure in leading to an overlap, or even to an inversion, of the Ψ^{+}_{LUMO} and Ψ^{-}_{HOMO} bands [35].

For M=Ni, the weakness of the M···M interactions with respect to the S···S repulsions will have two consequences. First, the Ψ^{+}_{LUMO} and Ψ^{-}_{HOMO} levels will not be far from each other. Second, since the dimerization will be weak, the nature of the donor will exert a stronger influence on the nature of both the intra and interdimer interactions. Consequently, the donor will have a strong control of the order and dispersion of the Ψ^{+}_{LUMO} and Ψ^{-}_{HOMO} bands. Because of the proximity of

the levels, even in the case that only one of the two bands is filled partially, there will be some band hybridization which will affect the details of the band dispersion and Fermi surface. A particularly revealing example is provided by α-(EDT-TTF)[Ni(dmit)$_2$] [36]. As shown in Fig. 12a, the Ψ^{+}_{LUMO} and Ψ^{-}_{HOMO} bands are found in the same energy range so that the resulting half-filled band has Ψ^{+}_{LUMO} character in some parts of the Brillouin zone but Ψ^{-}_{HOMO} character in some other [32]. Since the Ψ^{-}_{HOMO} band is 2D in nature whereas the Ψ^{+}_{LUMO} band is pseudo-1D (see the intended crossings in Fig. 12a), the resulting Fermi surface (Fig. 12b) calculated assuming a charge transfer of 1/2 electron per donor has both open and

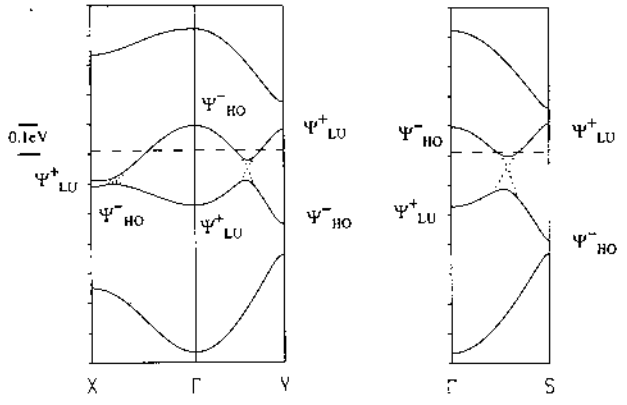

(a)

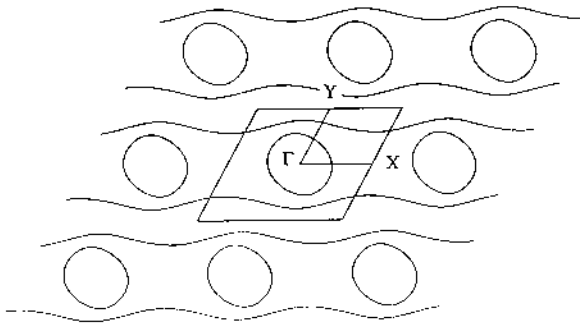

(b)

Fig. 12. (a) Dispersion relations calculated for the HOMO and LUMO bands of the EDTTTF slabs in α-(EDTTTF)[Ni(dmit)$_2$]. The dashed line refers to the Fermi level for a charge transfer of 1/2 electron per molecule. (b) Fermi surface associated with the band structure and Fermi level of Figure 12 a. Γ, X, Y and S refer to the wavevectors (0, 0); ($a^*/2$, 0); (0, $b^*/2$) and ($-a^*/2$, $b^*/2$), respectively.

closed portions. The real charge transfer and the origin of the resistivity anomaly of α-(EDT-TTF)[Ni(dmit)$_2$] are not known presently. It has been suggested [32] that the charge transfer could be of 1/2 electrons per donor and that the resistivity anomaly could originate from an instability of the EDT-TTF Fermi surface, although there is no experimental proof so far [37]. Whatever the real charge transfer and Fermi surfaces are, the results of Fig. 9 and Fig. 12 clearly prove that the donor molecules have a decisive influence in determining the character of the partially filled band in salts of Ni(dmit)$_2$ with dimeric building blocks. Again, it is clear that the situation is quite complex and that any serious attempt to understand the electronic structure of these salts needs a careful consideration of the role of both the HOMO *and* LUMO of Ni(dmit)$_2$.

An aspect worthy of comment for the Pd(dmit)$_2$ salts is the following. These salts may exhibit different physical behavior despite having quite similar structure. For instance, whereas Cs[Pd(dmit)$_2$]$_2$ [33] and δ-TTF[Pd(dmit)$_2$]$_2$ [25] are metallic at room temperature, (PMe$_4$)[Pd(dmit)$_2$]$_2$ [38] and β-(NMe$_4$)[Pd(dmit)$_2$]$_2$ [39] are room temperature semiconductors (although the second becomes metallic and even superconducting under pressure). In addition, even if both Cs[Pd(dmit)$_2$]$_2$ and δ-TTF[Pd(dmit)$_2$]$_2$ are room temperature metals and undergo a metal to insulator transition, the origin of the two transitions is different. X-ray diffuse scattering studies have shown that whereas the first one is a structural Peierls type transition [33] the second one happens without any structural change [40]. The band structure calculations for the Pd(dmit)$_2$ slabs of all these salts led to very similar results. All these observations led to the suggestion that the Mott-Hubbard interactions for these salts are of the same order as the Ψ^-_{HOMO} bandwidth and hence that the metallic and localized states are in strong competition. This is not so surprising if we remind that for all of these slabs there is an inversion of the Ψ^+_{LUMO} and Ψ^-_{HOMO} levels. This means that the interaction between the two Pd(dmit)$_2$ of the dimer is strong and consequently, that from an electronic viewpoint the essential building block of the slab is one dimer. If the charge transfer per Pd(dmit)$_2$ (ρ) is 1/2, we are in the situation where there is one electron per [Pd(dmit)$_2$]$_2$ dimer and thus, formally, in the same situation as for 1:1 charge transfer salts where one electron localizes in each unit of the lattice. Thus for Pd(dmit)$_2$ layers built from [Pd(dmit)$_2$]$_2$ dimers there should be a strong tendency for electron localization with one electron in each dimer. The difference with the usual 1:1 charge transfer salts is that since each unit of the layer contains two monomers, the intrasite electron repulsion (U) should be considerably smaller. Consequently, the localized state is not always the ground state as in the usual 1:1 charge transfer salts but is in competition with the metallic state.

It is clear that there are several ground states competing in these salts. Although the metallic state seems to be the more common, it is in strong competition with a localized state. Thus, cation disorder could have an important role in leading to an activated conductivity instead of the 'expected' metallic behavior. This is what presumably happens in (PMe$_4$)[Pd(dmit)$_2$]$_2$ and β-(NMe$_4$)[Pd(dmit)$_2$]$_2$. In cases like these, it is quite possible that the metallic state can be restored by applying pressure, as in β-(NMe$_4$)[Pd(dmit)$_2$]$_2$ [39]. For the room temperature metallic salts

there seems to be a strong tendency to undergo metal to semiconductor transitions, either through Mott–Hubbard or Fermi surface nesting mechanisms. Fine details of the crystal structure, like the degree of dimerization and counter-ion disorder, obviously have a very strong influence on the physical behavior of these salts.

3.2. Organic molecules versus transition metal complexes with similar shape

Here we will briefly explore another interesting use of transition metal complexes in making new molecular conductors by comparing some salts of the donors BEDT-TTF and $M(dddt)_2$ (see Fig. 3b, c). Several salts of $M(dddt)_2$, where M=Ni, Pd, Pt, Au and $dddt^{2-}$ is 5,6-dihydro-1,4-dithiin-2,3-dithiolato, have been prepared [41]. Because of the similarity between the two donors - in particular, because of the same shape of the molecule as well as the number and location of S and H atoms—it is expected that the intermolecular interactions in which the two donors will be engaged in salts with the same acceptor, will be very similar. This is not necessarily true when M=Pd or Pt because of the possibility of formation of metal–metal bonds, but most probably it will be the case for M=Ni. Thus, it can be expected that some of the BEDT-TTF and $Ni(dddt)_2$ salts can be isostructural. The metallic salt $[Ni(dddt)_2]_3(HSO_4)_2$ [42], is indeed isostructural with $(BEDT\text{-}TTF)_3(HSO_4)_2$ [43]. However, although both salts exhibit a metal to insulator transition, in the first case it occurs at a considerably lower temperature (25 K vs. 130 K). Thus, $[Ni(dddt)_2]_3(HSO_4)_2$ is a much more stable metal and this suggests that, despite the structural similarity, there can be important differences in their electronic structures. Thermopower measurements also have shown notable differences between the two salts.

The different behavior that isostructural salts of BEDT-TTF and $Ni(dddt)_2$ can exhibit is simple to understand. The HOMO and LUMO of $Ni(dddt)_2$ are similar in shape and energy separation with those of $Ni(dmit)_2$ [8,44]. However, the HOMO of BEDT-TTF lies very far apart from the LUMO, as usual for organic donors. Consequently, only the HOMO of the donor plays a major role in the conduction bands of the BEDT-TTF salts but both the HOMO and LUMO of the donor can be involved in those of the $Ni(dddt)_2$ salts. The calculated band structures near the Fermi level for the two salts $(BEDT\text{-}TTF)_3(HSO_4)_2$ and $[Ni(dddt)_2]_3(HSO_4)_2$ are shown in Fig. 13 [44,45]. The repeat unit of the donor slabs contains three molecules with an average charge of $+2/3$. The three bands of Fig. 13a are based mainly on the HOMO of BEDT-TTF. The three LUMO bands are quite far and are not shown in the drawing. This is not the case in the band structure of the $Ni(dddt)_2$ salt (see Fig. 13b). In that case there is no separation between the three HOMO and three LUMO bands. In both cases, the second and third bands from the bottom overlap. Since there are four electrons to fill the bands of Fig. 13, this leads to the metallic behavior of the two salts. A careful analysis of the bands of Fig. 13b shows that the lower part of the LUMO bands overlaps considerably with the upper part of the HOMO bands. Thus, via several avoided crossings, LUMO character is introduced in the HOMO bands of $[Ni(dddt)_2]_3(HSO_4)_2$. This is an important difference with respect to (BEDT-

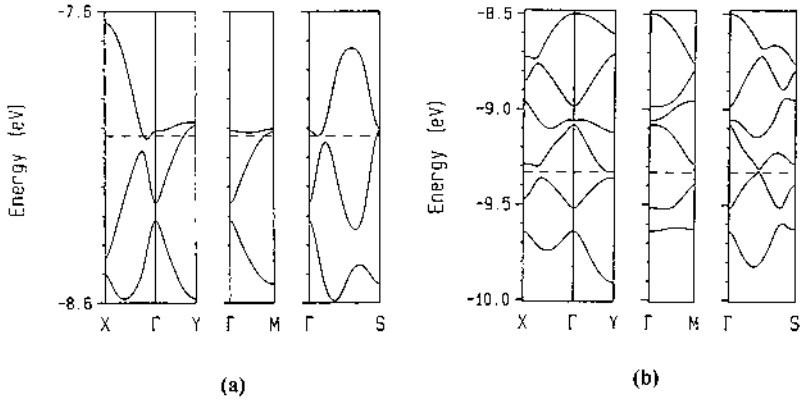

Fig. 13. Calculated band structure near the Fermi level (dashed line) for: (a) $(BEDT\text{-}TTF)_3(HSO_4)_2$ and (b) $[Ni(dddt)_2]_3(HSO_4)_2$.

$TTF)_3(HSO_4)_2$ for which the partially filled bands have almost exclusively HOMO character. Consequently, the shape of the Fermi surface is modified considerably [44] and thus it is expected that *the two salts will exhibit noticeable differences in their transport properties despite being isostructural.*

There is another important difference induced by the presence of a Ni atom in the central part of the donor which comes into play when trying to explain why $[Ni(dddt)_2]_3(HSO_4)_2$ is a more stable metal than $(BEDT\text{-}TTF)_3(HSO_4)_2$. As in other 3:2 salts where metallic conductivity is the result of the overlap between two bands, the more likely mechanism which could lead to the loss of the metallic properties is a lattice distortion which does not change the periodicity of the slab, yet, by changing some of the intermolecular interactions, suppresses the band overlap [44]. Let us note that whereas the band overlap is larger for the BEDT-TTF salt (which suggests that the metallic state should be stable until lower temperatures), the metal to insulator transition of the BEDT-TTF salt occurs at a considerably higher temperature. This can be understood if we take into account the relative stiffness of the two lattices. The donor slabs of the two salts can be considered to be build from parallel chains of trimeric units [42,43]. The mode of overlap between two such trimeric groups along the donor chains for the two isostructural salts is shown in Fig. 14a. Within a trimeric unit, the overlap mode allows the overlap between the

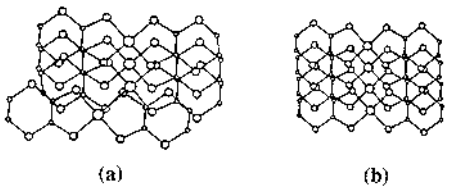

Fig. 14. Modes of overlap in: (a) $[Ni(dddt)_2]_3(HSO_4)_2$ (as well as $(BEDT\text{-}TTF)_3(HSO_4)_2$) and (b) $[Ni(dddt)_2]_3(AuBr_2)_2$.

Ni d orbitals and the S p orbitals of the planar five member rings. This leads to an additional source of stabilization of the lattice with respect to that of the BEDT-TTF salt. This stabilization mostly affects the filled levels of the system (i.e. it implicates filled $Ni(dddt)_2$ orbitals other than the HOMO, which have strong contributions from the metal), but these are the levels which contribute substantially to the cohesion energy of the lattice. This feature, absent in the BEDT-TTF salt because of the lack of d orbitals, makes the donor lattice of the $Ni(dddt)_2$ salt more rigid and consequently, the metal to insulator transition occurs at a lower temperature. Thus, *the use of the transition metal complex donor leads to a stabilization of the metallic state in this type of salts.*

Following the same reasoning, we expected that the rigidity of the lattice will increase and thus, the stability of the metallic state, if layers with larger units, (i.e. tetrameric, pentameric, etc.) could be prepared. The more favorable situation for the suppression of the metallic to insulator transition was thus expected to be found for donor layers containing uniform infinite chains of $Ni(dddt)_2$ donors instead of chains of trimeric units, as in $[Ni(dddt)_2]_3(HSO_4)_2$. This type of lattice has been reported recently [46] for the $[Ni(dddt)_2]_3(AuBr_2)_2$ salt (see Fig. 14b). Following our expectations, this salt retains the metallic properties down to at least 1.3 K [45].

4. Concluding remarks

There are many reasons why transition metal complexes are interesting to use as building blocks for new molecular conductors. The more obvious one is related to the large variety of shapes and charges they can afford. This is specially useful when the transition metal complex is just used as a counterion and does not participate in the conducting process. However, the more interesting situations arise when the transition metal complexes are those implicated in the conduction process. The fact that in the transition metal complex there is a metal atom coupling two (or more) organic ligands can lead to interesting variations in the electronic structure of molecular conductors with respect to those based on organic molecules.

Acknowledgements

This work was supported by the DGES-Spain Project PB96-0859 and Generalitat de Catalunya (1997 SGR 24). I am very pleased to thank L. Brossard for suggesting the study of the electronic structure of the $M(dmit)_2$ charge transfer salts. The work described here owes very much to collaborations over several years with P. Batail, K. Bechgaard, L. Brossard, P. Cassoux, D. Chasseau, M.-L. Doublet, O.A. Dyachenko, D. Jérome, J.P. Legros, I. Malfant, J.P. Pouget, I.E.-I. Rachidi, R. Rousseau, C. Rovira, S. Ravy, R.P. Shibaeva, A.E. Underhill, A. Vainrub, M.-H. Whangbo and E.B. Yagubskii.

References

[1] For some reviews see: (a) K. Krogmann, Angew. Chem. Int. Ed. Engl. 8 (1969) 35. (b) J.M. Williams, A.J. Schultz, A.E. Underhill, K. Carneiro, in: J.S. Miller (Ed.), Extended Linear Chain Compounds, Vol. 1, Plenum Press, New York, 1982, pp. 73–118. (c) A.E. Underhill, D.M. Watkins, J.M. Williams, K. Carneiro, in: J.S. Miller (Ed.), Extended Linear Chain Compounds, Vol. 1, Plenum Press, New York, 1982, pp. 119–156.

[2] (a) J. Ferraris, D.O. Cowan, V.V. Walatka, J.H. Perlstein, J. Am. Chem. Soc. 95 (1973) 948. (b) L.B. Coleman, M.J. Cohen, D.J. Sandman, F.G. Yamagishi, A.F. Garito, A.J. Heeger, Solid State Commun. 12 (1973) 1125.

[3] D. Jérome, A. Mazaud, M. Ribault, K. Bechgaard, J. Phys. Lett. (France) L41 (1980) 95.

[4] T. Ishiguro, K. Yamaji, Organic superconductors, Springer-Verlag, Berlin, 1990.

[5] L. Brossard, M. Ribault, M. Bousseau, L. Valade, P. Cassoux, C.R. Acad. Sci. Ser. II 302 (1986) 205.

[6] P. Cassoux, L. Valade, H. Kobayashi, A. Kobayashi, R.A. Clark, A.E. Underhill, Coord. Chem. Rev. 110 (1991) 115.

[7] P. Day, M. Kurmoo, J. Mater. Chem. 7 (1997) 1291.

[8] E. Canadell, New. J. Chem. 21 (1997) 1147.

[9] N.W. Ashcroft, N.D. Mermin, Solid State Physics, Holt, Rinehart and Winston, Philadelphia, 1985.

[10] E. Canadell, M.-H. Whangbo, Chem. Rev. 91 (1991) 965.

[11] N.F. Mott, Metal-insulator transitions, Barnes and Noble, NY, 1977.

[12] N. Thorup, G. Rindorf, H. Soling, K. Bechgaard, Acta Cryst. B37 (1981) 1236.

[13] B. Pommarède, B. Garreau, I. Malfant, L. Valade, P. Cassoux, J.-P. Legros, A. Audouard, L. Brossard, J.-P. Ulmet, M.-L. Doublet, E. Canadell, Inorg. Chem. 33 (1994) 3401.

[14] A. Pénicaud, P. Batail, K. Bechgaard, J. Sala-Pala, Synth. Met. 22 (1988) 201.

[15] C. Lenoir, K. Boubekeur, P. Batail, E. Canadell, P. Auban, O. Traetteberg, D. Jérome, Synth. Met. 41 (1991) 1939.

[16] E. Canadell, P. Batail, K. Boubekeur, M. Fourmigué (unpublished results).

[17] E. Canadell, Synth. Met. 70 (1995) 1009.

[18] E. Canadell, I.E.-I. Rachidi, S. Ravy, J.P. Pouget, L. Brossard, J.P. Legros, J. Phys. (France) 50 (1989) 2967.

[19] S. Ravy, J.P. Pouget, L. Valade, J.P. Legros, Europhys. Lett. 9 (1989) 391.

[20] A. Vainrub, E. Canadell, D. Jérome, P. Bernier, T. Nunes, M.-F. Bruniquel, P. Cassoux, J. Phys. (France) 51 (1990) 2465.

[21] L. Brossard, E. Canadell, L. Valade, P. Cassoux, Phys. Rev. B 47 (1993) 1647.

[22] Except otherwise stated all results reported in this work were obtained using a single-ζ basis set for the non metallic atoms and a double-ζ basis set for transition metal atoms. The calculations used an extended Hückel type hamiltonian (R. Hoffmann, J. Chem. Phys. 39 (1963) 1397. M.-H. Whangbo, R. Hoffmann, J. Am. Chem. Soc. 100 (1978) 6093) and the non diagonal H_{mn} matrix elements were calculated according to the modified Wolfsberg–Helmholtz formula (J.H. Ammeter, H.-B. Bürgi, J. Thibeault, R. Hoffmann, J. Am. Chem. Soc. 100 (1978) 3686).

[23] E. Canadell, S. Ravy, J.P. Pouget, L. Brossard, Solid State Commun. 75 (1990) 633.

[24] M. Bousseau, L. Valade, J.-P. Legros, P. Cassoux, M. Garbauskas, L.V. Interrante, J. Am. Chem. Soc. 108 (1986) 1908.

[25] J.-P. Legros, L. Valade, Solid State Commun. 68 (1988) 599.

[26] L. Brossard, M. Ribault, L. Valade, P. Cassoux, Phys. Rev. B 42 (1990) 3935.

[27] L. Brossard, M. Ribault, L. Valade, P. Cassoux, J. Phys. (France) 50 (1989) 1521.

[28] A recent study shows that upon lowering the temperature the closed Fermi surface opens and the nesting becomes better: S. Hebrard, D. Chasseau, J. Gaultier, I. Malfant, J.-P. Legros, M.-L. Doublet, E. Canadell, unpublished results. S. Hebrard, Thèse, Université de Bordeaux I, 1996.

[29] M.-L. Doublet, I. Malfant, S. Hebrard, E. Canadell, J. Gaultier, D. Chasseau, J.-P. Legros, L. Brossard, Acta Phys. Pol. A 87 (1995) 781.

[30] A. Kobayashi, A. Miyamoto, H. Kobyashi, R.A. Clark, A.E. Underhill, J. Mater. Chem. 1 (1991) 827.
[31] H. Kim, A. Kobayashi, Y. Sasaki, R. Kato, H. Kobayashi, Chem. Lett. (1987) 1799.
[32] M.-L. Doublet, E. Canadell, B. Garreau, J.-P. Legros, L. Brossard, P. Cassoux, J.P. Pouget, J. Phys. Condens. Matter 7 (1995) 4673.
[33] A.E. Underhill, R.A. Clark, I. Marsden, M. Allan, R.H. Friend, H. Tajima, T. Naito, M. Tamura, H. Kuroda, A. Kobayashi, H. Kobayashi, E. Canadell, S. Ravy, J.P. Pouget, J. Phys. Condens. Matter 3 (1991) 933.
[34] H. Tajima, M. Tamura, T. Naito, A. Kobayashi, H. Kuroda, R. Kato, H. Kobayashi, R.A. Clark, A.E. Underhill, Mol. Cryst. Liq. Cryst. 181 (1990) 233.
[35] See for instance: (a) R. Kato, Y.-L. Liu, H. Sawa, S. Aonuma, A. Ichikawa, H. Takahashi, N. Mori, Solid State Commun. 94 (1995) 973. (b) R. Kato, Y.-L. Liu, S. Aonuma, M. Sawa, Synth. Met. 96 (1997) 2087.
[36] R. Kato, H. Kobayashi, A. Kobayashi, T. Naito, M. Tamura, H. Tajima, H. Kuroda, Chem. Lett. (1989) 1839. H. Tajima, M. Inokuchi, A. Kobayashi, T. Ohta, R. Kato, H. Kobayashi, H. Kuroda, Chem. Lett. (1993) 1235.
[37] A. Kobayashi, A. Sato, K. Kawano, T. Naito, H. Kobayashi, T. Watanabe, J. Mater. Chem. 5 (1995) 1671.
[38] C. Faulmann, J.-P. Legros, P. Cassoux, J. Cornelissen, L. Brossard, H. Inokuchi, H. Tajima, M. Tokumoto, J. Chem. Soc. Dalton Trans. (1994) 249.
[39] A. Kobayashi, H. Kim, Y. Sasaki, K. Murata, R. Kato, H. Kobayashi, J. Chem. Soc. Faraday Trans. (1990) 361.
[40] S. Ravy, personal communication.
[41] E.B. Yagubskii, L.A. Kushch, V.V. Gritsenko, O.A. Dyachenko, L.I. Buravov, A.G. Khomenko, Synth. Met. 70 (1995) 1039.
[42] E.B. Yagubskii, A.I. Kotov, A.G. Khomenko, L.I. Buravov, A.I. Schegolev, R.P. Shibaeva, Synth. Met. 46 (1992) 255.
[43] L.C. Porter, H.H. Wang, M. Miller, J.M. Williams, Acta Crystallogr. C43 (1987) 2201.
[44] M.-L. Doublet, E. Canadell, J.P. Pouget, R.P. Shibaeva, J. Phys. I France 4 (1994) 1439.
[45] Note that the band structures of Fig. 13 were calculated [44] using double-ζ type orbitals for all atoms except H.
[46] L.A. Kushch, V.V. Gritsenko, L.I. Buravov, A.G. Khomenko, G.V. Shilov, O.A. Dyachenko, V.A. Merzhanov, E.B. Yagubskii, R. Rousseau, E. Canadell, J. Mater. Chem. 5 (1995) 1633.